

HIDDEN BROAD-LINE REGIONS IN SEYFERT 2 GALAXIES: FROM THE SPECTROPOLARIMETRIC PERSPECTIVE

PU DU¹, JIAN-MIN WANG^{1,2,3}, AND ZHI-XIANG ZHANG¹

¹Key Laboratory for Particle Astrophysics, Institute of High Energy Physics, Chinese Academy of Sciences, 19B Yuquan Road, Beijing 100049, China

²National Astronomical Observatories of China, Chinese Academy of Sciences, 20A Datun Road, Beijing 100020, China

³School of Astronomy and Space Science, University of Chinese Academy of Sciences, 19A Yuquan Road, Beijing 100049, China

ABSTRACT

The hidden broad-line regions (BLRs) in Seyfert 2 galaxies, which display broad emission lines (BELs) in their polarized spectra, are a key piece of evidence in support of the unified model for active galactic nuclei (AGNs). However, the detailed kinematics and geometry of hidden BLRs are still not fully understood. The virial factor obtained from reverberation mapping of type 1 AGNs may be a useful diagnostic of the nature of hidden BLRs in type 2 objects. In order to understand the hidden BLRs, we compile six type 2 objects from the literature with polarized BELs and dynamical measurements of black hole masses. All of them contain pseudobulges. We estimate their virial factors, and find the average value is 0.60 and the standard deviation is 0.69, which agree well with the value of type 1 AGNs with pseudobulges. This study demonstrates that (1) the geometry and kinematics of BLR are similar in type 1 and type 2 AGNs of the same bulge type (pseudobulges), and (2) the small values of virial factors in Seyfert 2 galaxies suggest that, similar to type 1 AGNs, BLRs tend to be very thick disks in type 2 objects.

Keywords: galaxies: active – galaxies: nuclei – galaxies: Seyfert – (galaxies:) quasars: emission lines

1. INTRODUCTION

The unified model (Antonucci 1993), which originates from the detection of broad emission lines (BELs) in the spectropolarimetric data of Seyfert 2 galaxy NGC 1068 (Antonucci & Miller 1985), proposes that the type 1 (showing both BELs and narrow emission lines) and type 2 (showing only narrow emission lines) active galactic nuclei (AGNs) are the same type of objects viewed from different angles. The hidden broad-line regions (BLRs) are observed in the polarized spectra of many type 2 AGNs (e.g., Antonucci 1984; Tran et al. 1992; Young et al. 1996; Moran et al. 2000; Ramos Almeida et al. 2016), and are thought to have scattering of BELs by the regions above the poles of accretion disks (called “polar scatter regions”) (Antonucci & Miller 1985; Antonucci 1993). However, the detailed geometry and kinematics of BLRs hidden in the centers of type 2 AGNs remain elusive and are not yet fully understood.

The virial mass of black holes can be obtained by reverberation mapping (RM, e.g., Blandford & McKee 1982; Peterson et al. 1998; Kaspi et al. 2000; Bentz et al. 2009; Du et al. 2014, 2015, 2016). The RM technique provides a key component, the time lag between continuum and BEL response, that provides a sizescale due to the finite speed of light. There is a dilemma that we are not able to get the black hole mass without specifying the kinematics and structure of the BLR. Fortunately, we can obtain the black hole mass from galactic dynamics in type 2 AGNs, providing the opportunity

to define the virial factor

$$f_{\text{vir}} = \frac{M_{\bullet}}{M_{\text{vir}}} = \frac{GM_{\bullet}}{V^2 R_{\text{BLR}}} \quad (1)$$

where M_{\bullet} is the BH mass determined by galactic dynamics techniques, M_{vir} is the virial mass, V is the width of BEL, R_{BLR} is the emissivity-weighted radius of BLR, G is the gravitational constant. For type 1 AGNs, $R_{\text{BLR}} = c\tau$, where c is the speed of light, τ is the time delay between the response of broad emission lines (mainly $H\beta$) to the variation of continuum which is normally measured from the peak of cross-correlation functions between the light curves of the continuum and emission lines. The value of virial factor is determined by the geometry and kinematics of BLR, and its evaluation leads to an indirect path to understand the nature of BLRs. Comparing statistically with the BH mass – stellar velocity dispersion ($M_{\bullet} - \sigma_{\ast}$) relation (e.g., Ferrarese & Merritt 2000; Tremaine et al. 2002), its average value is estimated as the order of unity for type 1 AGNs if the velocity V is measured from the full-width-half-maximum (FWHM) of broad $H\beta$ lines (e.g., Onken et al. 2004; Ho & Kim 2014; Woo et al. 2015). However, a more recent work indicates that the virial factor in individual objects probably varies significantly, as demonstrated by reconstructing the geometry and kinematics of BLRs in a small sample using the Markov Chain Monte Carlo method (MCMC, Pancoast et al. 2014). This result means that the kinematics of BLRs or the viewing angles are diverse in these objects.

The polar scattering regions in type 2 AGNs provides an additional viewing angle, namely from the polar axes, similar to the angle of observation for type 1 AGN. Considering

that the virial factor reflects the geometry and kinematics of BLRs, we can diagnose the hidden BLRs in type 2 AGNs by comparing the virial factors, obtained from their polarized spectra, to those of type 1 AGNs. Therefore, we search for type 2 AGNs with hidden BELs in polarized spectra and directly determined dynamical BH mass measurements, and estimate their f_{vir} factors.

2. VIRIAL FACTORS OF TYPE 2 AGNS

We compile all of the type 2 AGNs which have both polarized BEL detections and direct dynamical BH mass measurements from the published literatures in order to check their virial factors. The objects which are identified definitely as low-ionization nuclear emission-line regions (LINER, e.g., Ho 2008) or those with uncertain BH mass measurements have been eliminated. There are a total of six sources in the final sample. The degree of polarization in type 2 AGNs is generally very low (less than several percent), in most cases, only broad $H\alpha$ lines in the polarized spectra are visible (e.g., Antonucci 1984; Tran et al. 1992; Young et al. 1996; Moran et al. 2000; Ramos Almeida et al. 2016). We assume that broad $H\beta$ and $H\alpha$ lines have the same widths in the polarized spectrum for each individual object, as has been demonstrated in several objects (Ramos Almeida et al. 2016). Because the poor quality of polarized spectra would influence the measurements of the line dispersions (second momentum of the profile, σ), we only adopt the FWHM of polarized emission lines in the following analysis.

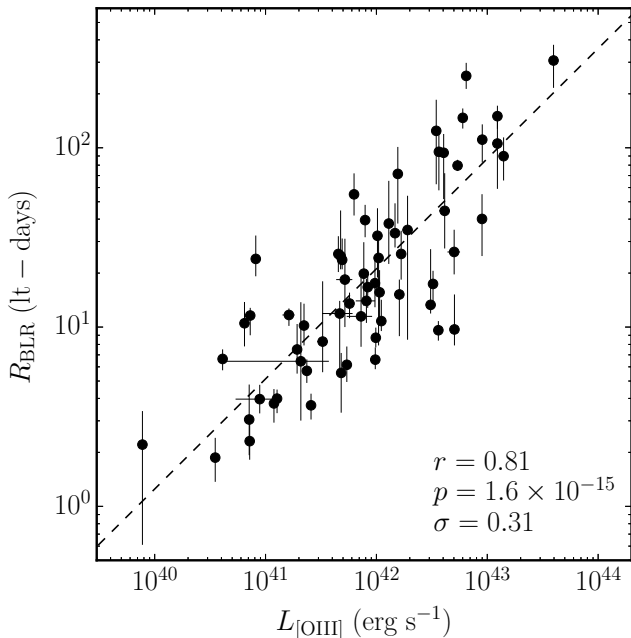


Figure 1. Correlation between the luminosity of [O III] and R_{BLR} . The points with error bars are the RM objects summarized in Du et al. (2015, 2016). The dotted line is the best fit. r is the Pearson’s correlation coefficient, p is null-probability of no correlation and σ is the standard deviation of residual after subtracting the best fit in logarithmic space. We adopt Λ CDM cosmology with $H_0 = 70 \text{ km s}^{-1} \text{ Mpc}^{-1}$, $\Omega_\Lambda = 0.7$ and $\Omega_M = 0.3$.

To estimate the radii of BLRs in Equation 1, instead of

the RM method as employed for type 1 AGNs, we use of two approaches: (1) the empirical relation between the time delay and the luminosity of [O III] λ 5007 and (2) the empirical relation with the hard X-ray luminosity in 2-10 keV found in the RM samples. For the first approach, we compile the luminosities of [O III] and the time delays of $H\beta$ for all of the type 1 AGNs that have RM observations summarized in Du et al. (2015, 2016). It should be noted that the narrow-line regions (NLRs) in type 1 AGNs suffer local extinction of $E(B-V) \sim 0.2 - 0.3$ (e.g., Netzer et al. 2006; Vaona et al. 2012) in addition to the Galactic extinction (Schlafly & Finkbeiner 2011). The line extinction should be corrected for the RM objects. Considering that the Balmer decrements of narrow lines for some RM objects are difficult to determine accurately because of their Lorentzian-like $H\alpha$ and $H\beta$ profiles (encompassing both narrow and broad components)¹, we adopt the mean $E(B-V)$ of 0.28, which is obtained from the Data Release 7 quasar sample of Sloan Digital Sky Survey (SDSS, Shen et al. 2011), to correct the intrinsic extinction in those RM objects. Using the FITEXY algorithm (Press et al. 1992) for linear regression, the resulting correlation (shown in Figure 1) is

$$\log R_{\text{BLR}} = -(24.475 \pm 0.684) + (0.614 \pm 0.016) \log L_{[\text{OIII}]}, \quad (2)$$

where $L_{[\text{OIII}]}$ is the extinction-corrected luminosity of [O III]. Equation 2 can be used to estimate the BLR radius. In order to avoid the potential contamination of star formation activities in [O III] fluxes, which would result in uncertainties in R_{BLR} estimates to some extent, we also adopt hard X-ray luminosity in 2-10 keV (L_{2-10} , the relation of L_{2-10} versus R_{BLR} in Kaspi et al. 2005) to deduce R_{BLR} as comparison. To calculate the virial factors of the hidden BLRs in type 2 AGN sample, their extinction in narrow emission lines and the absorption in 2-10 keV X-ray luminosities should be also taken into account (see the references in Table 1). The extinction-corrected [O III] luminosities (corrected individually using the Balmer decrement of NLR for each object found in the literatures) and absorption-corrected hard X-ray luminosities compiled from the literatures, as well as their deduced virial factors (denoted as $f_{[\text{OIII}]}$ and f_{2-10} , respectively), are listed in Table 1.

For the uncertainties of virial factors, the dispersions of the empirical relationships we used are included. For $f_{[\text{OIII}]}$, the primary uncertainties come from the dispersions of Equation 2 (0.31 dex, Figure 1). The uncertainties caused by the [O III] luminosity measurements are much smaller, and can be ignored. And we use the dispersion (62 percents) of the relation between L_{2-10} and R_{BLR} (Kaspi et al. 2005) to calculate the error bars of f_{2-10} . The uncertainties of L_{2-10} mainly result from their intrinsic variations over time, and have been rolled into the dispersion of the $L_{2-10} - R_{\text{BLR}}$

¹ The Lorentzian profiles of the entire $H\alpha$ and $H\beta$ emission lines and the too weak narrow lines for some PG quasars in Kaspi et al. (2000) and most of the AGNs with high accretion rates in Du et al. (2014, 2015, 2016) make it difficult to de-blend the narrow components from the broad components very reliably, and additionally, difficult to measure the reddening in their narrow-line regions using Balmer decrements.

relationship. Therefore, we do not include them explicitly.

Table 1. Virial factors

Object	FWHM(H α) (km s $^{-1}$)	Ref.	M_{\bullet} (M_{\odot})	Ref.	$\log L_{[\text{OIII}]}$ (erg s $^{-1}$)	Ref.	$f_{[\text{OIII}]}$	$\log L_{2-10}$ (erg s $^{-1}$)	Ref.	f_{2-10}
Circinus	2300 \pm 500	1	1.14 $^{+0.20}_{-0.20}$ $\times 10^6$	2	41.17	3	0.17 $^{+0.15}_{-0.15}$	42.62	4	0.20 $^{+0.16}_{-0.16}$
IC 2560	2100 \pm 300	1	2.51 $^{+3.80}_{-1.51}$ $\times 10^6$	5	40.19	6	1.83 $^{+3.11}_{-1.79}$	41.80	7	1.47 $^{+2.45}_{-1.34}$
NGC 1068	4377 \pm 300	8	8.39 $^{+0.44}_{-0.44}$ $\times 10^6$	9	42.38	4	0.06 $^{+0.05}_{-0.05}$	43.02	4	0.25 $^{+0.16}_{-0.16}$
NGC 2273	2399 \pm 419	10 ^b	8.61 $^{+0.91}_{-0.46}$ $\times 10^6$	11	41.13	4	1.28 $^{+1.02}_{-1.02}$	42.73	4	1.24 $^{+0.89}_{-0.89}$
NGC 3393	5000 \pm 600	1	1.57 $^{+0.98}_{-0.99}$ $\times 10^7$	12	42.04	3	0.15 $^{+0.14}_{-0.14}$	41.60	7	2.08 $^{+1.90}_{-1.91}$
NGC 4388	4500 \pm 1400	1	7.31 $^{+0.17}_{-0.18}$ $\times 10^6$	11	41.85	4	0.11 $^{+0.10}_{-0.10}$	42.90	4	0.24 $^{+0.21}_{-0.21}$

NOTE—References: 1. Ramos Almeida et al. (2016), 2. Greenhill et al. (2003), Kormendy & Ho (2013), 3. Bassani et al. (1999), 4. Marinucci et al. (2012), 5. Läsker et al. (2016), 6. Gu et al. (2006), 7. Tilak et al. (2008), 8. Inglis et al. (1995), 9. Lodato & Bertin (2003), Kormendy & Ho (2013), 10. Moran et al. (2000), 11. Kuo et al. (2011), Kormendy & Ho (2013), 12. Kondratko et al. (2008), Kormendy & Ho (2013). ^aThe Galactic and local extinction has been corrected. ^bWe measure the FWHM from the polarized spectrum in Ref. 10. We do not list the uncertainties of $L_{[\text{OIII}]}$ and L_{2-10} here, because we only use the dispersion of the empirical relationship to deduce the uncertainties of $f_{[\text{OIII}]}$ and f_{2-10} (see Section 2).

The comparison between the virial factors $f_{[\text{OIII}]}$ and f_{2-10} and their distributions are provided in Figure 2. The mean values of $f_{[\text{OIII}]}$ and f_{2-10} are 0.60 and 0.92, and their standard deviations are 0.69 and 0.73, respectively. The Kolmogorov – Smirnof test shows the probability is 8% (It means, if the two distributions were identical, they would appear as discrepant as the observations indicate by chance in 8% of the cases). Considering that the size of the present sample is quite small and the scatter is moderately large, we think the resulting $f_{[\text{OIII}]}$ and f_{2-10} in the present sample are not significantly inconsistent with each other². More observations are needed to clarify this point. The empirical relation between L_{2-10} and R_{BLR} we used to deduce f_{2-10} has more uncertainty (Kaspi et al. 2005), we prefer to use $f_{[\text{OIII}]}$ in the following discussion.

We individually corrected the extinction of $L_{[\text{OIII}]}$ for the six type 2 AGNs (see the references in Table 1), but we adopt a characteristic E(B-V) value to establish the $R_{\text{BLR}} - L_{[\text{OIII}]}$ relation for the RM AGNs. This characteristic correction method applies to a considerable size sample: (1) Adopting a characteristic value does not influence the slope of the $R_{\text{BLR}} - L_{[\text{OIII}]}$ relationship, because the Balmer decrement of NLR does not correlate with [O III] luminosity (Shen et al. 2011). (2) We have checked the effects of different characteristic extinctions, and find if we change it to 0.18 or 0.38, the $f_{[\text{OIII}]}$ only becomes 18% smaller or 22% larger, respectively. These uncertainties are much smaller than the error bars. We searched $(\text{H}\alpha/\text{H}\beta)_{\text{NLR}}$ for the RM sample, and found the values for 20 objects which can be measured from their narrow lines reliably (see Table 2). The median $(\text{H}\alpha/\text{H}\beta)_{\text{NLR}}$ for the 20 objects is 4.29, and the corresponding E(B-V) = 0.31 which is similar to the value (0.28) used

here. And also, 0.28 is consistent with the mean NLR extinction reported by Heard & Gaskell (2016) (see their Figure 3). Although we cannot find $(\text{H}\alpha/\text{H}\beta)_{\text{NLR}}$ reported for the entirety of the RM sample, there is no evidence that the average E(B-V) for the whole RM sample is significantly different from the value we used here. Therefore, the characteristic extinction is reasonable for the present sample.

Table 2. Balmer Decrements

Object	$(\text{H}\alpha/\text{H}\beta)_{\text{NLR}}$	Ref.
SDSS J075101.42+291419.1	6.16	1
Mrk 79	2.68	2

NOTE—References: 1. Obtained from the spectrum in SDSS, 2. Obtained from the spectrum in NASA/IPAC Extragalactic Database. (This table is available in its entirety in machine-readable form.)

3. COMPARISON WITH VIRIAL FACTOR IN TYPE 1 AGNS

In order to compare the obtained virial factors in the type 2 sample with the values in type 1 AGNs, we first provide some necessary background.

Once the time lag between continuum and emission line, as well as the emission line width, have been measured from RM, the mass of BH in an AGN can be determined using Equation 1 if the virial factor f_{vir} is known. Due to the fact that the velocity measurement could be either FWHM or σ , and the velocity could be measured from mean spectra or rms spectra (Peterson et al. 1998), there are four combinations of f_{vir} estimates (f_{vir} for FWHM in mean or rms spectra, or for σ in mean or rms spectra). For simplicity, we designate them as $f_{\text{FWHM}}(\text{mean})$, $f_{\text{FWHM}}(\text{rms})$, $f_{\sigma}(\text{mean})$ and $f_{\sigma}(\text{rms})$

² In fact, in the present sample, only $f_{[\text{OIII}]}$ and f_{2-10} of NGC 3393 looks different. The relatively anomalous behavior of NGC 3393 could be explained by the very large variation in its X-ray luminosity (see Figure 1 in Fabbiano et al. 2011).

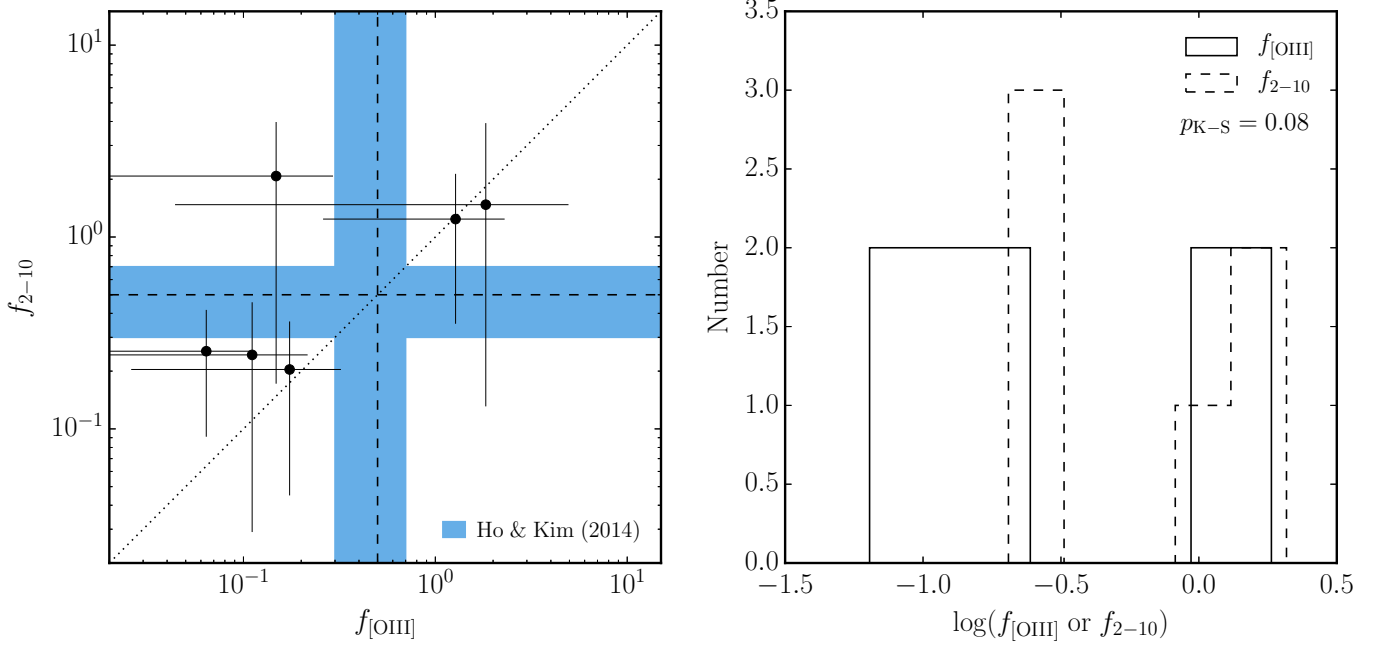


Figure 2. Virial factors. The left panel is the comparison between $f_{[\text{OIII}]}$ and f_{2-10} . The dashed lines and blue regions are the virial factor and its uncertainty for AGNs with pseudobulges in [Ho & Kim \(2014\)](#). The dotted line is the diagonal. The right panel shows the distributions of $f_{[\text{OIII}]}$ and f_{2-10} (solid lines for $f_{[\text{OIII}]}$ and dashed lines for f_{2-10}). p_{K-S} is the Kolmogorov – Smirnov probability (see Section 2).

Assuming the velocity distribution of BLR is isotropic (which is likely not true), the simplest deduction from theory is that the virial factor for FWHM is 0.75 ([Netzer 1990](#)). Observationally, the average virial factor for a sample can be calibrated by comparing the RM objects with measurements of bulge stellar velocity dispersion with the $M_{\bullet} - \sigma_{*}$ relation of inactive galaxies, if we assume that active and inactive galaxies follow the same $M_{\bullet} - \sigma_{*}$ relation. Based on a sample of 14 AGNs with RM observations, [Onken et al. \(2004\)](#) calibrated $f_{\text{FWHM}}(\text{rms}) = 1.4$ and $f_{\sigma}(\text{rms}) = 5.5$ through the comparison with the $M_{\bullet} - \sigma_{*}$ relation from [Ferrarese & Merritt \(2000\)](#) and [Tremaine et al. \(2002\)](#). By adding the observations from Lick AGN Monitoring Project (LAMP, e.g., [Bentz et al. 2009](#)), [Woo et al. \(2010\)](#) compiled a sample of 24 RM objects with σ_{*} measurements and found that $\log f_{\sigma}(\text{rms}) = 0.72^{+0.09}_{-0.10}$, if adopting the $M_{\bullet} - \sigma_{*}$ relation in [Gültekin et al. \(2009\)](#), which is in good agreement with the value of [Onken et al. \(2004\)](#). [Graham et al. \(2011\)](#) improved the $M_{\bullet} - \sigma_{*}$ relation by including more BH mass measurements of barred galaxies, and derived $f_{\sigma}(\text{rms}) = 3.8^{+0.7}_{-0.6}$, which is lower than the value in [Woo et al. \(2010\)](#) by a factor of 2, for their sample of 28 AGNs. When dividing the sample into barred and non-barred galaxies, they found $f_{\sigma}(\text{rms})$ would be $2.3^{+0.6}_{-0.5}$ and $7.0^{+1.8}_{-1.4}$, respectively. Furthermore, they accounted for the selection bias caused by the non-detection of intermediate-mass BHs, and gave $f_{\sigma}(\text{rms}) = 2.8^{+0.7}_{-0.5}$, $2.3^{+0.9}_{-0.6}$ and $5.4^{+1.5}_{-1.2}$ for full, barred and non-barred AGN samples. [Park et al. \(2012\)](#) claimed that the discrepancy of virial factors in those previous works is mainly caused by the sample selection effect, and preferred to use $\log f_{\sigma}(\text{rms}) = 0.71 \pm 0.11$. [Woo et al. \(2013\)](#) investigated the assumption that active and inactive

galaxies follow the same $M_{\bullet} - \sigma_{*}$ relation, and demonstrated it is generally reasonable. [Grier et al. \(2013\)](#) updated the RM sample, and added new σ_{*} measurements of a few highly-luminous quasars. They obtained $f_{\sigma}(\text{rms}) = 4.31 \pm 1.05$ which is slightly lower than Park et al.’s value but larger than that in [Graham et al. \(2011\)](#). Motivated by the fact that galaxies with pseudobulges do not obey the $M_{\bullet} - \sigma_{*}$ relation of classical bulges and ellipticals, [Ho & Kim \(2014\)](#) separated the calibration by bulge types in galaxies and provided calibrated values of $[f_{\text{FWHM}}(\text{mean}), f_{\sigma}(\text{mean}), f_{\text{FWHM}}(\text{rms}), f_{\sigma}(\text{rms})] = [1.3 \pm 0.4, 5.6 \pm 1.3, 1.5 \pm 0.4, 6.3 \pm 1.5]$ for classical bulges and ellipticals, and $[0.5 \pm 0.2, 1.9 \pm 0.7, 0.7 \pm 0.2, 3.2 \pm 0.7]$ for pseudobulges. More recently, [Woo et al. \(2015\)](#) used the single-epoch spectra and the $R_{\text{BLR}} - L_{5100}$ relationship to calibrate narrow-line Seyfert 1 galaxies, and found $\log f_{\text{FWHM}}(\text{mean}) = 0.05 \pm 0.12$ and $\log f_{\sigma}(\text{mean}) = 0.65 \pm 0.12$.

Based on another technology, [Pancoast et al. \(2014\)](#) carried out MCMC to reconstruct kinematics models of BLRs in five Seyfert 1 galaxies. It does not rely on $M_{\bullet} - \sigma_{*}$ relation, but uses RM data only and can provide f_{vir} estimates for individual objects. Adopting this an independent method, [Pancoast et al. \(2014\)](#) derives the averages f_{vir} for the five objects to be ≈ 0.85 and ≈ 4.74 corresponding for FWHM and σ , respectively. However, the values in individual objects are very different (by an order of magnitude). They also showed that f_{vir} strongly depends on the inclination angle of the BLR and is much larger in more face-on objects (from ~ 0.2 for the viewing angle of 50 degrees to ~ 6 for 10

degrees)³.

For the present Seyfert 2 sample, it is difficult to measure the σ of emission lines accurately in their polarized spectra given the poor signal-to-noise ratio (σ depends on accurate measurement of the wings of emission lines). However, FWHMs are more robustly measured. We only estimate the virial factors based on FWHM. The average value of f_{vir} in those Seyfert 2s is 0.60, and the dispersion is 0.69. Considering that all of the objects in the sample are galaxies with pseudobulges (Kormendy & Ho 2013), this number is in good agreement with the $f_{\text{FWHM}}(\text{mean})$ and $f_{\text{FWHM}}(\text{rms})$ for Seyfert 1 galaxies with pseudobulges in Ho & Kim (2014). Therefore, we can draw a preliminary conclusion, based on the present type 2 sample of limited size, that the virial factors in type 2 AGNs are consistent with the values in type 1 AGNs of the same bulge type (pseudobulge).

Scattering regions in type 2 AGNs are mainly located along the polar axis (e.g., Antonucci 1983; Capetti et al. 1995), and provide a new perspective to BLRs from pole-on direction (small viewing angles). The similar value of virial factors, which are found from the polarized spectra of type 2 AGNs, as in type 1 objects indicate that the geometry and kinematics of BLR are similar in type 1 and type 2 AGNs of the same bulge type (pseudobulge). And the small virial factors ($f_{[\text{O III}]} = 0.60$) found from the polarized spectra demonstrate that the geometry of BLRs in the present sample tend to be very thick disks (thicker than the results in Pancoast et al. 2014 because of our smaller f_{vir}) or are perhaps even isotropic to some extent.

It should be noted that thermal motion of the free electrons in scattering regions could provide an additional broadening to the polarized emission lines, and further, influence the estimates of virial factors to some extent. Miller et al. (1991) shows that, consistent with the conclusion of Antonucci & Miller (1985), thermal electrons dominate the scattering process in NGC 1068 and broaden the polarized emission lines. Unfortunately, similar information is unavailable in other AGNs. On the other hand, lower temperature dust grains could also contribute to the scattering,

and may dominate at least in some objects. In such case, the additional broadening from the scattering particles is not an issue. The virial factor of NGC 1068 is low compared to the other 5 objects (Table 1). If the width from the dust scattering were used, it would be more similar. The detailed nature of scattering and the corresponding broadening still remain open questions and need to be investigated in the future.

4. SUMMARY

In this work we compile a sample of six Seyfert 2 galaxies with spectropolarimetric observations and dynamical BH mass measurements, and derive their virial factors from the FWHMs of the polarized BELs, in order to investigate the kinematics and geometry of hidden BLRs in type 2 AGNs. Generally, the virial factors estimated in the different ways (from the luminosities of [O III] and X-ray) are in agreement. The average of the derived virial factors is 0.60 in the present sample, which is similar to the value of type 1 objects with pseudobulges (Ho & Kim 2014). It implies that (1) the geometry and kinematics of BLR are similar in type 1 and type 2 AGNs of the same bulge type (pseudobulge) and (2) the geometry of BLRs in type 2 AGNs tend to be a very thick disk or isotropic. In the future, more spectropolarimetric observations would make it possible to explore the properties of hidden BLRs in more details, and further, to investigate the dependency of hidden BLR kinematics and geometry on black hole masses or accretion rates of AGNs.

We acknowledge the support of the staff of the Lijiang 2.4m telescope. Funding for the telescope has been provided by CAS and the People's Government of Yunnan Province. This research is supported by NSFC grants NSFC-11503026, -11173023, and -11233003, and a NSFC-CAS joint key grant U1431228, by the CAS Key Research Program through KJZD-EW-M06, by National Key Program for Science and Technology Research and Development (grant 2016YFA0400701), and by Key Research Program of Frontier Sciences, CAS, Grant NO. QYZDJ-SSW-SLH007.

REFERENCES

- Antonucci, R. R. J. 1983, *Nature*, 303, 158
 Antonucci, R. R. J. 1984, *ApJ*, 278, 499
 Antonucci, R. 1993, *ARA&A*, 31, 473
 Antonucci, R. R. J., & Miller, J. S. 1985, *ApJ*, 297, 621
 Bassani, L., Dadina, M., Maiolino, R., et al. 1999, *ApJS*, 121, 473
 Bentz, M. C., Walsh, J. L., Barth, A. J., et al. 2009, *ApJ*, 705, 199
 Blandford, R. D., & McKee, C. F. 1982, *ApJ*, 255, 419
 Capetti, A., Axon, D. J., Macchetto, F., Sparks, W. B., & Boksenberg, A. 1995, *ApJ*, 446, 155
 Du, P., Hu, C., Lu, K.-X., et al. (SEAMBH Collaboration) 2014, *ApJ*, 782, 45
 Du, P., Hu, C., Lu, K.-X., et al. (SEAMBH Collaboration) 2015, *ApJ*, 806, 22
 Du, P., Lu, K.-X., Zhang, Z.-X., et al. (SEAMBH Collaboration) 2016, *ApJ*, 825, 126
 Fabbiano, G., Wang, J., Elvis, M., & Risaliti, G. 2011, *Nature*, 477, 431
 Ferrarese, L., & Merritt, D. 2000, *ApJL*, 539, L9
 Graham, A. W., Onken, C. A., Athanassoula, E., & Combes, F. 2011, *MNRAS*, 412, 2211
 Greenhill, L. J., Booth, R. S., Ellingsen, S. P., et al. 2003, *ApJ*, 590, 162
 Grier, C. J., Martini, P., Watson, L. C., et al. 2013, *ApJ*, 773, 90
 Gu, Q., Melnick, J., Cid Fernandes, R., et al. 2006, *MNRAS*, 366, 480
 Gültekin, K., Richstone, D. O., Gebhardt, K., et al. 2009, *ApJ*, 698, 198
 Heard, C. Z. P., & Gaskell, C. M. 2016, *MNRAS*, 461, 4227
 Ho, L. C. 2008, *ARA&A*, 46, 475
 Ho, L. C., & Kim, M. 2014, *ApJ*, 789, 17
 Inglis, M. D., Young, S., Hough, J. H., et al. 1995, *MNRAS*, 275, 398
 Kaspi, S., Maoz, D., Netzer, H., et al. 2005, *ApJ*, 629, 61
 Kaspi, S., Smith, P. S., Netzer, H., et al. 2000, *ApJ*, 533, 631
 Kormendy, J., & Ho, L. C. 2013, *ARA&A*, 51, 511
 Kondratko, P. T., Greenhill, L. J., & Moran, J. M. 2008, *ApJ*, 678, 87
 Kuo, C. Y., Braatz, J. A., Condon, J. J., et al. 2011, *ApJ*, 727, 20

³ It should be noted that, besides the inclination angle, the thickness of BLR and some other dynamical parameters also influence the virial factor. Also Pancoast et al. (2014) reported that 4 of 5 objects show very thick BLRs, only the BLR of Mrk 1310 is relatively thin.

- Läsker, R., Greene, J. E., Seth, A., et al. 2016, *ApJ*, 825, 3
- Lodato, G., & Bertin, G. 2003, *A&A*, 398, 517
- Marinucci, A., Bianchi, S., Nicastro, F., Matt, G., & Goulding, A. D. 2012, *ApJ*, 748, 130
- Miller, J. S., Goodrich, R. W., & Mathews, W. G. 1991, *ApJ*, 378, 47
- Moran, E. C., Barth, A. J., Kay, L. E., & Filippenko, A. V. 2000, *ApJL*, 540, L73
- Netzer, H. 1990, *Active Galactic Nuclei*, 57
- Netzer, H., Mainieri, V., Rosati, P., & Trakhtenbrot, B. 2006, *A&A*, 453, 525
- Onken, C. A., Ferrarese, L., Merritt, D., et al. 2004, *ApJ*, 615, 645
- Pancoast, A., Brewer, B. J., Treu, T., et al. 2014, *MNRAS*, 445, 3073
- Park, D., Kelly, B. C., Woo, J.-H., & Treu, T. 2012, *ApJS*, 203, 6
- Peterson, B. M., Wanders, I., Bertram, R., et al. 1998, *ApJ*, 501, 82
- Press, W. H., Teukolsky, S. A., Vetterling, W. T., & Flannery, B. P. 1992, Cambridge: University Press, —c1992, 2nd ed.,
- Ramos Almeida, C., Martínez González, M. J., Asensio Ramos, A., et al. 2016, *MNRAS*, 461, 1387
- Schlafly, E. F., & Finkbeiner, D. P. 2011, *ApJ*, 737, 103
- Shen, Y., Richards, G. T., Strauss, M. A., et al. 2011, *ApJS*, 194, 45
- Tilak, A., Greenhill, L. J., Done, C., & Madejski, G. 2008, *ApJ*, 678, 701-711
- Tran, H. D., Miller, J. S., & Kay, L. E. 1992, *ApJ*, 397, 452
- Tremaine, S., Gebhardt, K., Bender, R., et al. 2002, *ApJ*, 574, 740
- Vaona, L., Ciroi, S., Di Mille, F., et al. 2012, *MNRAS*, 427, 1266
- Woo, J.-H., Schulze, A., Park, D., et al. 2013, *ApJ*, 772, 49
- Woo, J.-H., Treu, T., Barth, A. J., et al. 2010, *ApJ*, 716, 269
- Woo, J.-H., Yoon, Y., Park, S., Park, D., & Kim, S. C. 2015, *ApJ*, 801, 38
- Young, S., Hough, J. H., Efstathiou, A., et al. 1996, *MNRAS*, 281, 1206